# Upregulation of C/EBPα Inhibits Suppressive Activity of Myeloid Cells and Potentiates Antitumor Response in Mice and Cancer Patients

#3128

Ayumi Hashimoto[1*], Debashis Sarker[2*], Vikash Reebye[3*], Sheba Jarvis[3], Mikael H Sodergren[3], Andrew Kossenkov[1], Nina Raulf[4], Jenni Vasara[4], Pinelopi Andrikakou[3], Tim Meyer[5], KaiWen Huang[6], Ruth Plummer[7], Cheng E Chee[8], Duncan Spalding[3], Madhava Pai[3], David J Pinato[3], Rohini Sharma[3], Bristi Basu[9], Daniel Palmer[10], Yuk-Ting Ma[11], Robert Habib[4], Anna Martirosyan[12], Naouel Elasri[12], Adeline Reynaud[12], John J. Rossi[13], Mark Cobbold[14], Nagy A Habib[3,4], Dmitry I. Gabrilovich[14]

## Background

Transcriptional factors regulating the function of myeloid cells represent an attractive targeting opportunity due to their broad effect on the function of these cells. The transcription factor CCAAT/enhancer-binding protein alpha (C/EBPα) is involved in differentiation of myeloid cells, proliferation, metabolism, and immunity. Deregulation of C/EBPα has been reported in several solid tumors including liver, breast and lung. We have developed a first-in-class small activating RNA therapeutic comprising a SMARTICLES® liposomal nanoparticle encapsulating CEBPA-51, a 2'O-Me RNA oligonucleotide duplex designed to specifically target and up-regulate transcription of the CEBPA gene. The mechanism of antitumor effect of MTL-CEBPA, as well as its possible effect in cancer patients remains unclear.

## Effect of MTL-CEBPA on LLC Tumor Growth and Myeloid Function in Mice

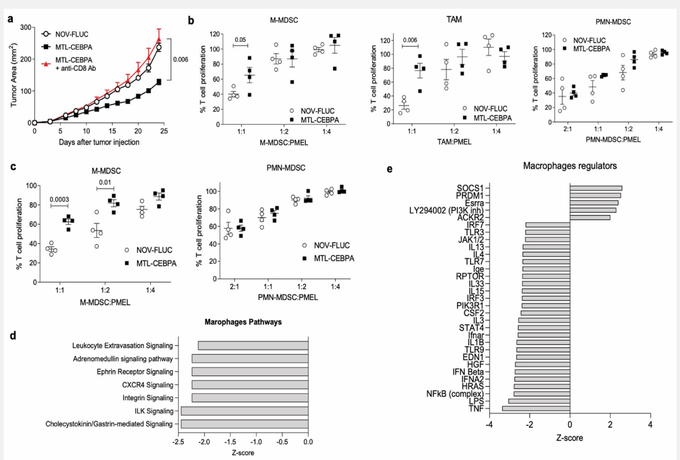


**The effect of MTL-CEBPA on LLC tumor growth and myeloid cell function.**

MTL-CEBPA and control NOV-FLUC were intravenously injected to the tumor-bearing mice at 3 mg/kg twice a week from Day 5. **a)** Kinetics of LLC tumor growth in the mice depleted of CD8 T cells and treated with MTL-CEBPA (n = 5 per group). Mean and SD are shown. P values were calculated in two-way ANOVA. **b)** Suppression of T cell proliferation by M-MDSC, macrophage and PMN-MDSC isolated from the tumors of the LLC tumor-bearing mice treated with NOV-FLUC or MTL-CEBPA for 2 weeks (n = 4). **c)** Suppression of T cell proliferation by M-MDSC and PMN-MDSC isolated from the spleens of the LLC tumor-bearing mice treated with NOV-FLUC or MTL-CEBPA for 2 weeks (n = 4). Mean and SD are shown. P values were calculated in two-sided Student's t-test. TAM and PMN-MDSC were isolated from the tumors of LLC-tumor bearing mice treated with NOV-FLUC or MTL-CEBPA for 2 weeks and used for RNAseq analysis. **d)** Pathways predicted to be inhibited (z-score < -2) in TAM in MTL-CEBPA as compared to NOV-FLUC treated groups. **e)** Regulators predicted to be activated (z-score > 2) or inhibited (z-score < -2) in TAM in MTL-CEBPA as compared to NOV-FLUC treated groups.

## Mechanism of MTL-CEBPA Regulation in Myeloid Cells in Mice

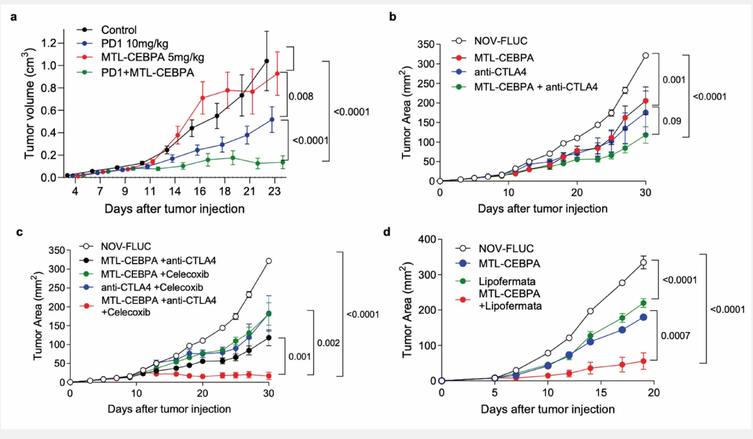


**Therapeutic efficacy of MTL-CEBPA in combination with immunotherapies.**

**a)** the MC38 tumor-bearing mice were intravenously treated with MTL-CEBPA or NOV-FLUC control at 5 mg/kg from Day 4 (twice a week). Anti-PD1 antibody was intraperitoneally injected to the mice twice a week at 10 mg/kg. **b)** The LLC tumor-bearing mice were intravenously treated with MTL-CEBPA or NOV-FLUC control at 3 mg/kg from Day 3 (twice a week). Anti-CTLA4 antibody was intraperitoneally injected to the mice on Days 10, 17 and 24 (100 μg/mouse). Celecoxib was orally treated to the mice at 50 mg/kg from Day 3 (daily). **c)** The LLC tumor-bearing mice were intravenously treated with MTL-CEBPA or NOV-FLUC (3 mg/kg from Day 3, twice a week) in combination with lipofermata (2 mg/kg, twice per day from Day 3, subcutaneously). In each experiment p values were calculated in two-way ANOVA.

## Mechanism of MTL-CEBPA Regulation in Human Myeloid Cells

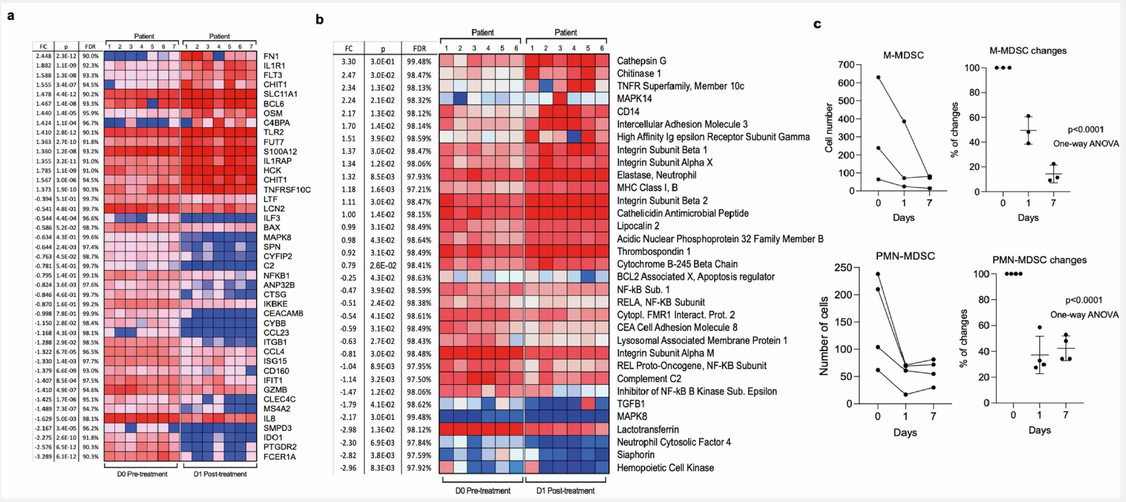


**Effect of MTL-CEBPA treatment (alone) of patients with HCC on gene and protein expression in myeloid cells.**

**a)** Gene expression profile evaluated by NanoString® using the human PanCaner IO 360 panel. Heat map of gene expression up regulated (+1 > $\log_2$ fold change and above) or downregulated (-1 < $\log_2$ fold change and below) with a false discovery rate (FDR) of < 5% is shown. **b)** Protein expression profile evaluated by mass spectroscopy. Proteins with p value < 0.05 and absolute $\log_2$ fold change > 1 were considered as significantly differentially expressed. Adjusted p values were calculated by correcting for a false discovery rate (FDR) of < 5%. **c)** The presence of M-MDSC (CD66b$^-$ CD14$^+$ HLA-DR$^{-/lo}$CD15$^-$ CD11b$^+$CD38$^+$) and PMN-MDSC (CD66b$^+$CD14$^-$CD15$^+$CD11b$^+$ LOX1$^+$) cells among mononuclear cells were analysed by flow cytometry.

## Efficacy of MTL-CEBPA in Combination with Sorafenib in Patients with Liver Cancer

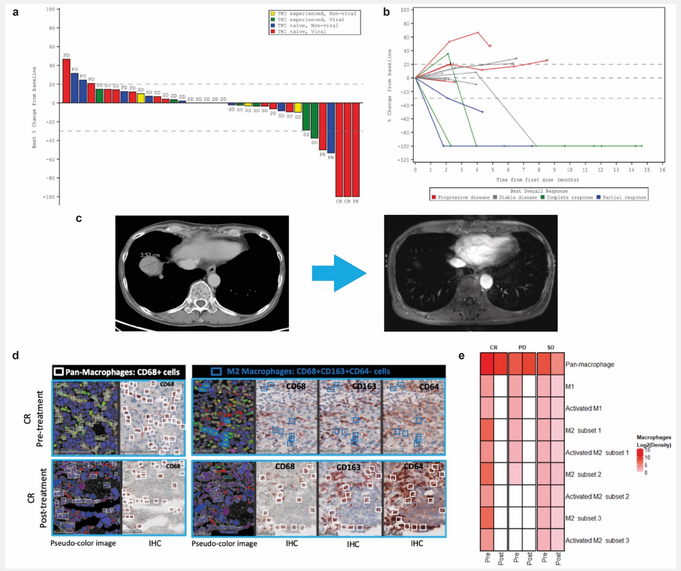


**Clinical activity of MTL-CEBPA in advanced HCC patients treated in combination with sorafenib.**

**a)** Waterfall plot of patients in Phase 1b study showing best % change from baseline, with identification of groups that had previously been treated with TKI and those that had HCC of viral etiology (cutoff date May 1st, 2020). **b)** Durable responses of patients previously naïve to TKI with HCC of viral etiology. Spider plot in Phase 1b patients who had not previously been treated with TKI and had HCC of viral etiology, showing tumor response for target lesions. **c)** Complete radiological response of lung metastases following treatment with MTL-CEBPA and Sorafenib. Cross-sectional imaging of patient with baseline imaging on top from June 12th, 2018 showing right lung metastases and on bottom from December 31st, 2018 showing complete resolution of lung metastases. Patient maintains a complete radiological response to both liver and lung metastases on last surveillance imaging March 13th, 2020. **d)** Representative images of CR patients' biopsies with a complete loss of pro-tumoral M2 macrophages (blue squares: CD68$^+$CD163$^+$CD64$^-$ cells). White squares represent the Pan-macrophage population expressing CD68. Pseudo-color image: created by virtual slides alignment and imported in Halo software for biomarkers analysis. **e)** Heatmap of macrophage subsets set up based on $\log_2$ fold change between pre- and post-treatment (cell densities) samples of 3 HCC patients: Complete responder (CR), Stable Disease (SD) and Progressive Disease (PD). Following macrophage populations were analyzed: Pan-Macrophage (CD68$^+$ cells), Anti-tumoral M1 macrophages (CD68$^+$CD64$^+$CD163$^-$CD206$^-$ cells), Activated M1 macrophages (CD68$^+$CD64$^+$CD163$^-$CD206$^-$ cells), Pro-tumoral M2 macrophages subset 1 (CD68$^+$CD163$^+$CD64$^-$ cells), Pro-tumoral M2 macrophages subset 2 (CD68$^+$CD206$^+$CD64$^-$ cells), Pro-tumoral M2 macrophages subset 3 (CD68$^+$CD163$^+$CD206$^+$CD64$^-$ cells), Activated M2 subsets characterized by IL-10 production.

## Author Affiliation

[1]Wistar Institute, Philadelphia, PA, US
[2]Kings College London, London, UK
[3]Imperial College London, London, UK,
[4]MiNA Therapeutics Ltd, London, UK
[5]University College London Cancer Institute, London, UK
[6]National Taiwan University, Taipei, Taiwan
[7]Northern Centre for Cancer Care and Newcastle University, UK
[8]National University Cancer Institute Singapore, Singapore
[9]University of Cambridge, Cambridge, UK
[10]University of Liverpool & Clatterbridge Cancer Centre, Liverpool, UK
[11]University of Birmingham and University Hospitals Birmingham NHS Trust, Birmingham, UK
[12]HalioDx, Marseille, France
[13]Department of Molecular and Cellular Biology, Beckman Research Institute of City of Hope, Duarte, USA
[14]AstraZeneca, Gaithersburg, MD, USA
*considered joint first authors